Measurement of the impact-parameter dependent azimuthal anisotropy in coherent ρ^0 photoproduction with ALICE

A. G. Riffero (for the ALICE Collaboration)
University and INFN Torino, Italy

Coherent vector meson photoproduction in ultraperipheral heavy-ion collisions is a well-established tool to probe the gluon structure of the colliding nuclei. We will focus on the observation of quantum interference effects in the ρ^0 meson photoproduction, in the form of angular anisotropy. Such an anisotropy appears due to two different factors: first, the photons involved in the process are linearly polarized along the impact parameter, and, second, quantum interference occurs between the two amplitudes that contribute to the ρ^0 photoproduction cross section. Furthermore, the interference effect strongly depends on the impact parameter of the collision, which acts as the distance between the openings of a two-slit interferometer. We present the first measurement of this anisotropy in coherent ρ^0 photoproduction from ultraperipheral Pb–Pb collisions at a center-of-mass energy of $\sqrt{s_{\mathrm{NN}}} = 5.02$ TeV per nucleon pair, as a function of the impact parameter of the collision. The latter is estimated by classifying the events in nuclear-breakup classes defined by neutron emission. The ρ^0 mesons are detected by the ALICE experiment through their decay into a pion pair. The anisotropy occurs as a function of ϕ, defined as the azimuth angle between the two vectors formed by the sum, and the difference, of the transverse-momentum of the pions, respectively. It results in a $\cos(2\phi)$ modulation of the photoproduced ρ^0; the amplitude of the modulation is found to increase by about one order of magnitude from large to small impact parameters. This trend is compatible with the available theoretical predictions.

DOI: https://doi.org/10.17161/p17qpn24
Keywords: coherent photoproduction, ρ^0, azimuthal anisotropy, impact parameter

1 Introduction

Ultra-peripheral collisions (UPCs) occur when the impact parameter of the collision is greater than the sum of the radii of the colliding nuclei. In UPCs, due to the short range of the strong force, purely hadronic interactions are highly suppressed, allowing one to study photon-induced processes [1, 2, 3, 4]. In these interactions the electric charges of the colliding nuclei work coherently and produce an intense electromagnetic field, that can be described in terms of a flux of quasi-real photons.

Of great interest is the photoproduction of a vector meson, that is a well established tool to probe the gluon structure of the colliding nuclei. In this process one of the nuclei emits a photon that fluctuates into a quark–antiquark color dipole, which interacts strongly with the other nucleus and appears as a real vector meson. The photo-nuclear interaction can be either coherent, if the photon couples with the whole nucleus, or incoherent if it couples with only one nucleon. These processes can be disentangled using the transverse momentum of the produced vector meson, that is related to the size of the target in the impact-parameter plane, and it is of the order of 60 (500) MeV/c in the coherent (incoherent) case.

In the coherent case, it is not known which of the nuclei emits the photon and which acts as the target in the interaction, opening up the possibility to study, at femtometer scales, the fundamental quantum mechanical interference between the amplitudes [5]. At the Large Hadron Collider (LHC), the photoproduction process occurs through the exchange of a Pomeron, a color-neutral two-gluon state at lowest order. This restricts the production site within one of the two nuclei, therefore this process can be seen as a double slit experiment at fm scale, where the impact-parameter acts as the distance between the openings of the interferometer. In Ref [5] it is also shown that the interference effect involved should be stronger at mid-rapidity, where the two amplitudes are almost the same, and at small impact parameter.

The strong electromagnetic fields in UPCs of heavy ions can cause multiple photon exchanges in a single collision. These additional photons usually lead to independent electromagnetic dissociation (EMD) processes accompanying the coherent vector meson photoproduction. These EMD processes are useful because they allow one to select different impact parameter ranges [6], always remaining ultra-peripheral, by means of neutrons emitted at beam rapidities by the excited nuclei.

Experimentally, the emitted neutrons can be detected using two zero-degree calorimeters (ZDCs) each of them covering the direction of one of the incoming colliding nuclei. UPCs can therefore be classified as: (*i*) 0n0n, if no neutrons are detected in the ZDCs, (*ii*) Xn0n + 0nXn, if at least one neutron is detected in only one of the ZDCs, and (*iii*) XnXn, if both ZDCs have neutron signal. For brevity, the Xn0n + 0nXn class will be denoted as Xn0n in the following. The intensity of the electromagnetic field decreases with increasing impact parameter. XnXn events, where at least three photons are exchanged, are dominated by relatively small impact parameters. Xn0n events select a broader impact-parameter range than XnXn, while 0n0n events cover all possible impact parameters. EMD is modeled in the RELDIS [7, 8] and **n$_\mathbf{O}^\mathbf{O}$n** [9] models, while the coherent production of vector mesons accompanied by electromagnetic dissociation is studied with **n$_\mathbf{O}^\mathbf{O}$n** and STARlight [10].

Since the electromagnetic fields of the colliding nuclei are highly Lorentz-contracted, the exchanged photons are fully linearly polarized. In Ref. [11] it has been proposed that due to this polarization the interference effect can give rise to an azimuthal anisotropy in the di-lepton production from photon-photon fusion. This effect has also been studied as a function of the impact parameter in Ref. [12], and measured, for XnXn events by the STAR Collaboration in Au–Au UPCs at $\sqrt{s_{\mathrm{NN}}}\ =\ 200$ GeV [13].

These studies were later extended to the photoproduction of a ρ^0 vector meson, where the ρ^0 inherits the linear polarization of the photon. The interference correlates momentum and polarization, ensuring that the anisotropy of the decay of a spin-1 particle into two spin-less products is preserved when averaging over events with random impact parameters. The anisotropy here is predicted to manifest as a $\cos(2\phi)$ asymmetry [14, 15], where the angle ϕ is defined as the angle between the two vectors formed by the sum and by the difference of the p_{T} of the pions produced in the decay $\rho^0 \to \pi^+\pi^-$.

The predicted $\cos(2\phi)$ asymmetry has been measured by the STAR Collaboration, for coherent ρ^0 photoproduction in XnXn events, in Au–Au and U–U UPCs at $\sqrt{s_{\mathrm{NN}}}\ =\ 200$ GeV and $\sqrt{s_{\mathrm{NN}}}\ =\ 193$ GeV, respectively [16]. This asymmetry has also been recently studied by the CMS Collaboration using exclusive diffractive production of jets at the LHC [17].

Here, we report the first measurement of the impact-parameter dependence of the $\cos(2\phi)$ asymmetry in Pb–Pb UPCs at $\sqrt{s_{\mathrm{NN}}}\ =\ 5.02$ TeV using the coherent photoproduction of a ρ^0 meson. The ρ^0 meson is detected through its decay into a pion pair at midrapidity. The strength of the anisotropy is measured in three different EMD classes (0n0n, Xn0n, and XnXn) that select different impact parameter ranges.

2 Experimental set-up

A full description of the ALICE apparatus and its performance is given in Refs. [18, 19]. We present in the following a brief description of the sub-detectors involved in the measurement presented in this analysis. The pion tracks are reconstructed using the Inner Tracking System (ITS) [20], a six-layer silicon tracker coaxial to the beam line, and the Time Projection Chamber (TPC) [21], a big gaseous detector that surrounds the ITS. The two innermost layers of the ITS form the Silicon Pixel Detector (SPD), that is also used for triggering. The TPC provides also particle identification, via the measurement of the specific ionization energy loss.

The V0 [22] and ALICE Diffractive (AD) [23] detectors, located at forward rapidities, are formed by scintillator arrays on both sides of the interaction point (IP) and provide a veto, suppressing hadronic interactions.

The impact parameter ranges mentioned in Sec. 1 are selected by detecting the neutrons emitted at forward rapidity, using the Zero Degree Calorimeters. There are two ZDC detectors for neutrons, one per side of the IP, that have an energy resolution good enough to be sensitive to the emission of a single neutron.

The analyzed data were collected by ALICE in 2015, during the Run 2 of the LHC, using Pb–Pb collisions at $\sqrt{s_{\mathrm{NN}}}\ =\ 5.02$ TeV, and a dedicated UPC trigger. This trigger is formed by five different signals: four of them veto any activity of the AD or V0 detector within the time window for nominal beam–beam interactions, to suppress hadronic collisions. The fifth signal is a topological trigger that selects events that have at least two track segments [24] in the SPD, with an opening angle in azimuth greater than 153 degrees. This topology was chosen since the tracks of the pions are almost back-to-back in azimuth, due to the very small transverse momentum of coherently produced ρ^0. The integrated luminosity of the sample, determined using the V0 detectors as explained in Ref. [24], is about 485 mb^{-1}.

3 Data analysis

3.1 Event and track selection

The events selected for the analysis were required to have good-quality tracks. A track is considered good if (*i*) it has more than 50 associated TPC clusters, (*ii*) has been reconstructed in both ITS and TPC and matches the track segments in the SPD that fired the trigger, and (*iii*) has a distance of closest approach to the event primary vertex smaller than $0.0182 + 0.0350/(p_{\mathrm{T}}^{\mathrm{trk}})^{1.01}$ cm in the transverse plane and smaller than 2 cm in the longitudinal direction, where $p_{\mathrm{T}}^{\mathrm{trk}}$ is the transverse momentum, in GeV/c, associated to the track.

The passing event were required to fulfill additional selections: (*i*) have exactly two opposite-sign tracks, (*ii*) have no offline reconstructed signal in neither the V0 nor AD detectors, and (*iii*) fulfill the pion selection $\mathrm{n}_{\sigma 1}^2 + \mathrm{n}_{\sigma 2}^2 < 5^2$, where $\mathrm{n}_{\sigma 1}$ ($\mathrm{n}_{\sigma 2}$) is the difference, in units of the TPC ionization energy loss resolution, between the measured energy loss for track 1 (track 2) and the expected value for a pion with the same momentum.

Kinematic selections were also applied: (*i*) the pion pair rapidity must lie in the range $|y| < 0.8$ to avoid acceptance edge effects, (*ii*) the invariant mass of the pion pair must be inside the range $0.6\ \mathrm{GeV}/c^2 < m_{\pi\pi} < 0.95\ \mathrm{GeV}/c^2$, and (*iii*) the transverse momentum (p_{T}) of the ρ^0 candidate must be less than 0.1 GeV/c to select coherent processes with high purity. Using these selection criteria, the contamination from incoherent events is found to be lower than 4% [24]. More details about event and track selections can be found in Ref. [24].

3.2 ϕ definition

The observable used to measure the azimuthal anisotropy described in Sec. 1 is the azimuth angle ϕ, defined through the transverse momentum of the pions into which the ρ^0 decays. The ϕ angle can be defined in two different ways, indicated, respectively, as *average* and *charge*. In both cases ϕ is the angle between the transverse components of $\vec{p}_+$ and $\vec{p}_-$, where $\vec{p}_\pm = \vec{\pi}_1 \pm \vec{\pi}_2$. Using the *charge* definition, $\vec{\pi}_1$ and $\vec{\pi}_2$ are, respectively, the momentum of the positive and of the negative track. Using the *average* definition, $\vec{\pi}_{1,2}$ are randomly associated to the positive or to the negative track. The *average* definition, that by construction does not allow for a $\cos(\phi)$ component, has been used as default, while the *charge* definition has been used in the evaluation of systematic uncertainties.

3.3 Monte Carlo corrections

A Monte Carlo (MC) simulation, using the STARlight MC generator and a realistic description of the ALICE detector has been used to estimate the correction for acceptance and efficiency ($\mathrm{Acc} \times \epsilon$) to detect the pion tracks. This simulation describes the raw data kinematics well, with the exception of the transverse momentum distribution [25]. In order to improve the agreement between MC and data, a re-weighting procedure has been applied to the generated p_{T}^2 spectrum. The procedure consists of two steps: the first is to fit the inclusive pion pair p_{T}^2 distribution of the generated MC using the function:

$$\frac{\mathrm{d}N}{\mathrm{d}p_{\mathrm{T}}^2} = c \mid F(\mid t \mid,\ a_{\mathrm{Pb}},\ R_{\mathrm{Pb}}) \mid^2, \tag{1}$$

where c is a normalization constant and $F(\mid t \mid)$ is the form factor of the lead nucleus, obtained as a numerical approximation of the Fourier transform of a Wood-Saxon function [26, 27], and R_{Pb} and a_{Pb} are fit parameters. This is possible since for sufficiently high transverse momentum, p_{T}^2 can be approximated with the Mandelstam variable t. The second step is to obtain the weights using

$$\mathrm{w}(p_{\mathrm{T}}) = \frac{\mid F(\mid t \mid,\ a_{\mathrm{Pb}},\ R_{\mathrm{X}}) \mid^2}{\mid F(\mid t \mid,\ a_{\mathrm{Pb}},\ R_{\mathrm{Pb}}) \mid^2}, \tag{2}$$

where a_{Pb} is fixed to the fit result and R_{X} is chosen in such a way that, after applying the weights to each event of a given generated p_{T}, the reconstructed p_{T}^2 spectrum in the MC best reproduces the one in the data. This is achieved by minimizing the bin-by-bin difference between the p_{T} distributions of data and reconstructed MC as a function of R_{X}, using a χ^2-like variable. It was verified that the same R_{X} can be used to reproduce the data in all ϕ bins, therefore the weights were computed using the integrated data sample.

The Acc $\times$ ϵ correction was obtained using the STARlight MC simulations by computing the ratio of reconstructed to generated number of pion pairs in each invariant mass and ϕ interval, after applying the weights discussed above at the generation level. The raw invariant mass spectra of pion pairs, for each invariant mass and ϕ interval, was then divided by Acc $\times$ ϵ, to obtain the corrected mass spectra.

3.4 Signal extraction

The corrected mass spectra, in each neutron class and in each ϕ bin, were fitted using a modified Söding model [28] to extract the different contributions to the production of pion pairs. The fitting function is

$$\frac{dN}{dm_{\pi\pi}} = \mid A \cdot BW_{\rho} + B \mid^2 + n_{\mu\mu}\, M(m_{\pi\pi}), \tag{3}$$

where $m_{\pi\pi}$ is the pion pair invariant mass, BW_{ρ} is the relativistic Breit-Wigner shape that describes the ρ^0, A is its amplitude and B is the amplitude of the continuum pion pair production. The last term models the background originating from muons produced in the $\gamma\gamma \to \mu^+\mu^-$ process that have been misidentified as pions, with a shape $M(m_{\pi\pi})$ estimated with a dedicated MC, based on the STARlight generator, and the normalization constant $n_{\mu\mu}$ as a parameter of the fit. As discussed in Ref. [24], it was verified that the contribution from the ω decay is negligible since the ρ^0 yield does not vary significantly if it is not fixed to zero.
The relativistic Breit-Wigner function describing the ρ^0 resonance is:

$$BW_{\rho} = \frac{\sqrt{m_{\pi\pi} \cdot m_{\rho} \cdot \Gamma_{\rho}(m_{\pi\pi})}}{m_{\pi\pi}^2 - m_{\rho}^2 + i \cdot m_{\rho} \cdot \Gamma_{\rho}(m_{\pi\pi})} \tag{4}$$

and its width is:

$$\Gamma_{\rho}(m_{\pi\pi}) = \Gamma(m_{\rho}) \cdot \frac{m_{\rho}}{m_{\pi\pi}} \cdot \left(\frac{m_{\pi\pi}^2 - 4m_{\pi}^2}{m_{\rho}^2 - 4m_{\pi}^2}\right)^{3/2}. \tag{5}$$

The fits were performed by fixing the pole mass m_{ρ} and the pole width $\Gamma(m_{\rho})$ of the ρ^0 to the values reported for a ρ^0 formed in a photoproduction reaction, namely, $m_{\rho} = 769.2$ MeV/c^2 and $\Gamma(m_{\rho}) = 151.5$ MeV/c^2 [29]. A default strategy was chosen to extract the central value of the asymmetry parameter. In this strategy, the *average* definition of ϕ is used and the background contribution is fixed to zero in the invariant mass fits. Different strategies were explored and are used for the systematic uncertainty evaluation. To check the robustness of the fit procedure, the fit of the invariant mass distribution were repeated 100 times, using each time a different binning and fit ranges; the lower limit of the fit range was varied from 0.6 to 0.65 GeV/c^2, and the upper limit from 0.9 to 0.95 GeV/c^2. An example of the mass fits, performed with the default strategy for a specific ϕ interval and for the 0n0n and XnXn classes, is shown in Fig. 1. After the fit, the ρ^0 yield is obtained by integrating the signal function $|A\, BW_{\rho}|^2$ in the mass range $0.6 < m_{\pi\pi}$ (GeV/c^2) < 0.95. Such a range was chosen to be consistent with the STAR measurement [16] and with available theory calculations (see Sec. 4 for details).

3.5 Asymmetry extraction

The extraction of the amplitude of the modulation is affected by the migration of events between neutron classes, due to detector efficiency and pile-up effects, as discussed in Ref. [24]. To take this into account, a simultaneous fit to the ρ^0 yield as a function of ϕ in all three classes (0n0n, Xn0n, XnXn) was performed, using the following expression:

$$\begin{pmatrix} n_{\rho\,\mathrm{0n0n}(\phi)} \\ n_{\rho\,\mathrm{Xn0n}(\phi)} \\ n_{\rho\,\mathrm{XnXn}(\phi)} \end{pmatrix} = \begin{pmatrix} 1 \\ 1 \\ 1 \end{pmatrix} + \begin{pmatrix} w_{\,\mathrm{0n0n} \to \mathrm{0n0n}} & w_{\,\mathrm{Xn0n} \to \mathrm{0n0n}} & w_{\,\mathrm{XnXn} \to \mathrm{0n0n}} \\ w_{\,\mathrm{0n0n} \to \mathrm{Xn0n}} & w_{\,\mathrm{Xn0n} \to \mathrm{Xn0n}} & w_{\,\mathrm{XnXn} \to \mathrm{Xn0n}} \\ w_{\,\mathrm{0n0n} \to \mathrm{XnXn}} & w_{\,\mathrm{Xn0n} \to \mathrm{XnXn}} & w_{\,\mathrm{XnXn} \to \mathrm{XnXn}} \end{pmatrix} \begin{pmatrix} a_{2\,\mathrm{0n0n}} \\ a_{2\,\mathrm{Xn0n}} \\ a_{2\,\mathrm{XnXn}} \end{pmatrix} \cos(2\phi), \tag{6}$$

where $n_{\rho\,\mathrm{0n0n}}$ is the normalized ρ^0 yield in a given ϕ range for the 0n0n class, and similarly for other classes, and the fitting parameters $a_{2\,\mathrm{0n0n}}$, $a_{2\,\mathrm{Xn0n}}$ and $a_{2\,\mathrm{XnXn}}$ are the amplitudes of the $\cos(2\phi)$ modulation in the three classes. The coefficients $w_{\,\mathrm{Y} \to \mathrm{Z}}$ represent the contribution of the physical neutron class Y to the yield in the experimental neutron class Z, computed using the measured cross sections and migration probabilities as determined in Ref. [24]. The constant term is fixed to unity by normalization.

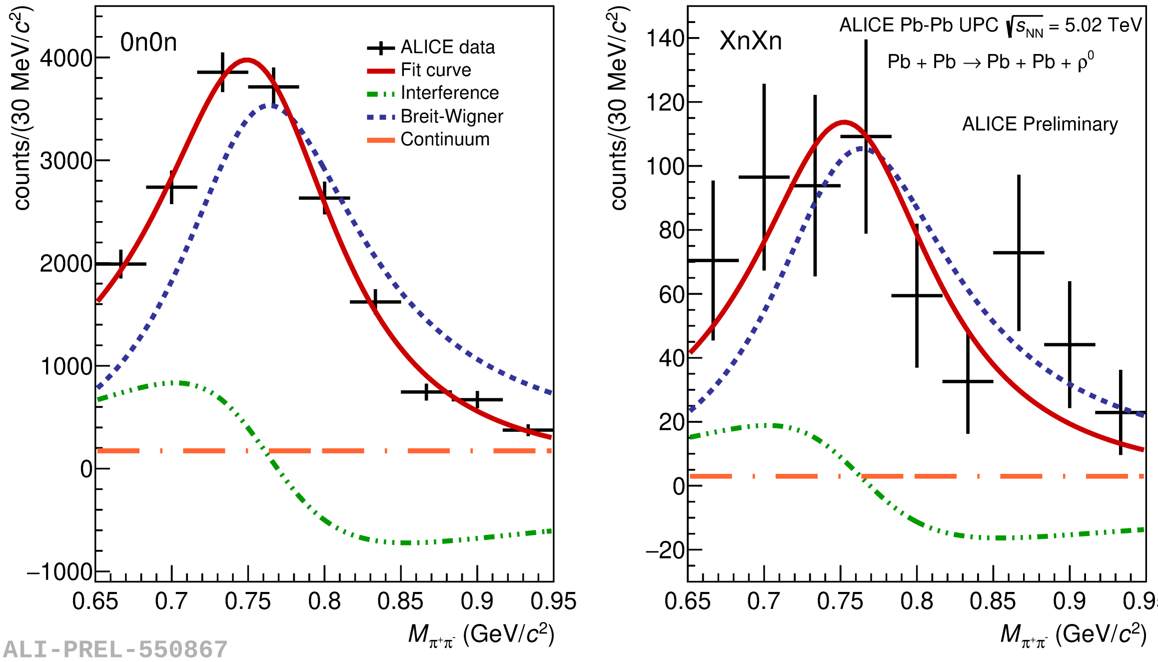

Figure 1 – Invariant-mass distribution of pion pairs, with a superimposed Söding fit, for the range $36^\circ < \phi < 60^\circ$, and for the default strategy discussed in the text, in the 0n0n (left) and XnXn (right) neutron classes. The different components of the pion-pair production amplitude are shown: the Breit-Wigner shape that describes the ρ^0 (dotted line), the continuum process (dash-dotted line), and the interference between the ρ^0 and the continuum (dash-dot-dot-dot line).

This simultaneous fitting procedure is repeated 100 times, on the different distributions of the ρ^0 as a function of ϕ provided by the signal extraction procedure explained in Sec. 3.4. An example of this simultaneous fit is shown in Fig. 2.

In each class, the central value of modulation has been taken as the mean value of the distribution of the amplitude, and the statistical uncertainty has been evaluated as the mean value of the distribution of the uncertainties from the fit.

3.6 Systematic uncertainties

The systematic uncertainties affecting the results presented here can be grouped in two categories: signal extraction and Acc $\times\ \epsilon$.

The systematic uncertainty related to the signal extraction has three contributions. The first has been evaluated as the standard deviation of the distribution of the $\cos(2\phi)$ amplitudes over the 100 trials mentioned above. The second contribution comes from using an alternative model, by Ross and Stodolsky [30], to fit the invariant mass distributions, and has been evaluated as the difference between the amplitudes obtained using the two models. The third contribution was estimated using different strategies for the measurement of the ρ^0 yield as a function of ϕ. The considered strategies include using the *charge* or *average* definition of ϕ, and setting or not the muon background to zero in the mass fits. Note that, in *charge* mode, the ρ^0 yield as a function of ϕ may have a $\cos(\phi)$ component [31], which was added to the fit function of Eq. 6. This may or may not be done for the *average* mode, resulting in six different possible strategies (including the default one). The systematic uncertainty due to the choice of a strategy has been evaluated as the difference between the result obtained with the default strategy and the mean value of results obtained with the others.

The systematic uncertainty on the Acc $\times\ \epsilon$ mainly arises from the re-weighting procedure described in Sec. 3.3. It was obtained by using, instead of the R_X value that minimizes the χ^2, the two values of R_X for which the χ^2 increases by one unit with respect to the minimum. The systematic uncertainty is estimated as the larger difference, in each class and for the default strategy, between the results obtained with the original and with the modified sets of weights. As a consistency check, it was also verified that, when the analysis is performed in rapidity sub-ranges containing roughly half of the total number of events, the extracted amplitudes are all compatible with each other within one standard deviation.

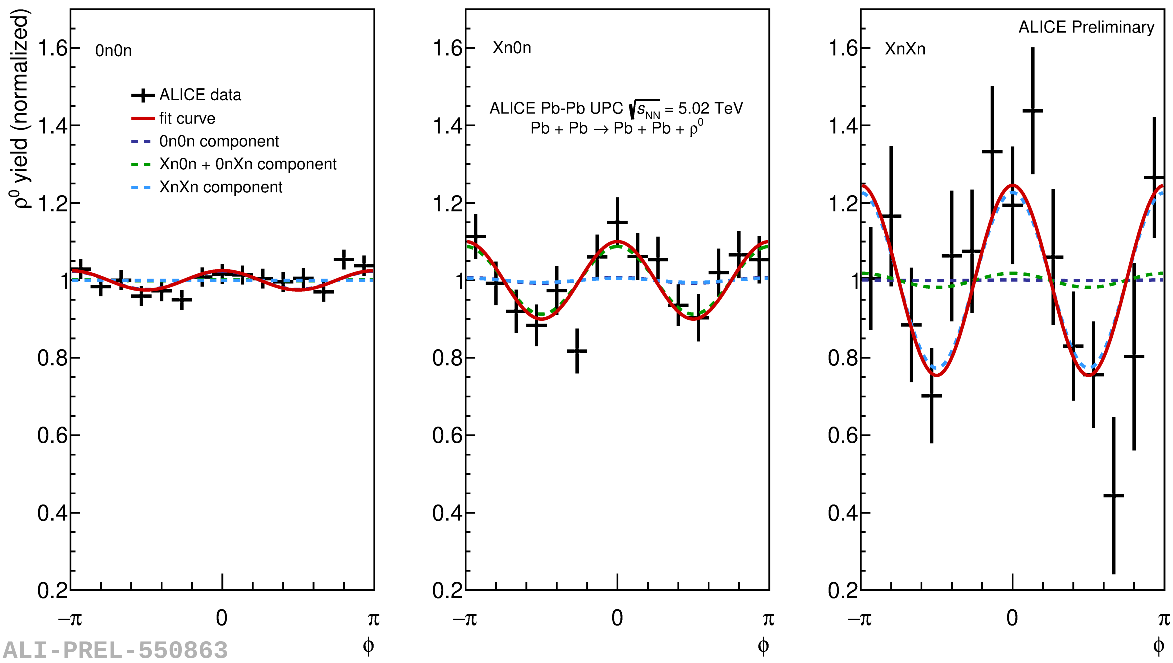

Figure 2 – Example of a simultaneous fit used to extract the amplitude of the $\cos(2\phi)$ modulation in all neutron classes. The contribution of each physical class to the yield in all experimental classes is shown.

4 Results

Figure 3 shows the extracted amplitude of the $\cos(2\phi)$ modulation as a function of the neutron class. The measured anisotropy shows a clear trend, with a significant increase, by approximately one order of magnitude, from 0n0n to XnXn, which according to **n$_\mathbf{O}^\mathbf{O}$n** corresponds to a variation of the median impact parameter between, approximately, 49 and 18 fm. Similar values can be obtained also using the analytical model presented in Ref. [32]; similar values for XnXn are also reported in Ref. [6]. We quote the median, instead of the mean, impact parameter because it is less sensitive to a tail of interactions extending to very large impact parameters [32].

As discussed in Sec. 1, the $\cos(2\phi)$ anisotropy in the model emerges from the presence of two elements: (i) the photon is linearly polarized along the impact parameter and this polarization is transferred to the produced vector meson, (ii) the two amplitudes that contribute to the cross section of the vector meson photoproduction process interfere.

The results are compared with the models by H. Xing *et al.* [14] and by W. Zhao *et al.* [33]. In the H. Xing *et al.* model, the quasi-real photon exchanged by the nuclei is treated as a color quark–antiquark dipole, that recombines to produce a ρ^0 after scattering off the color glass condensate state [34] inside the nuclei. The model from W. Zhao *et al.* uses the same formalism of the H. Xing *et al.* model, with two main differences: (i) the interaction of the quark–antiquark dipole with the target is implemented by computing the corresponding Wilson lines, and (ii) the color charge density used to obtain the Wilson lines is varied event-by-event to represent the different possible color configurations of the target.

The uncertainty of the model by H. Xing *et al.* [14] mostly comes from the probability of emitting a neutron from the scattered nucleus at a given impact parameter, where this latter has been estimated using three different parametrization from Refs. [35, 36, 37]. The model prediction is compatible with data for all neutron classes. In the model by W. Zhao *et al.* [33] the quoted uncertainty originates from the statistical precision from the finite number of sampled configurations. The predictions of this model also give a reasonable description of data, with the possible exception of the 0n0n class.

For the XnXn class, the ALICE result is also compared with the ones from the STAR Collaboration [16], for Au–Au and U–U collisions at a lower center-of-mass energy of $\sqrt{s_{\rm NN}} = 200$ GeV and $\sqrt{s_{\rm NN}} = 193$ GeV, respectively. The amplitude measured by ALICE is compatible with both STAR results. This is consistent with the models, which predict the $\cos(2\phi)$ modulation amplitude to vary with the colliding nuclei and the center-of-mass energy by less than the current experimental uncertainties.

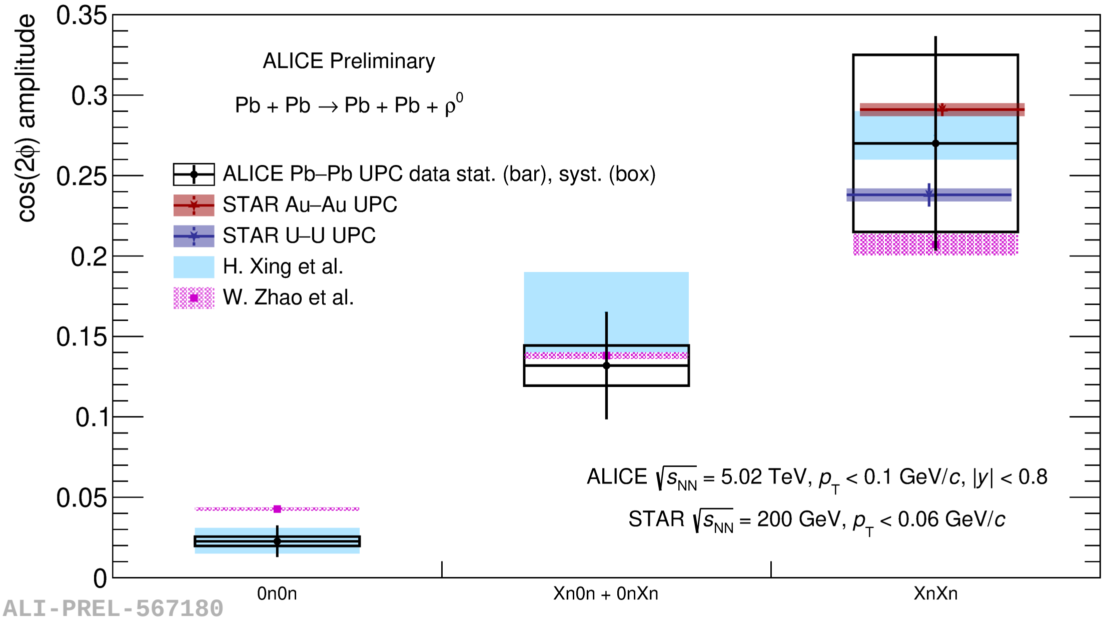

Figure 3 – Amplitudes of the $\cos(2\phi)$ modulation of the ρ^0 yield as a function of the neutron class, compared with the Xing *et al.* [14] and W. Zhao *et al.* [33] model predictions and, for XnXn, with the STAR results [16].

5 Conclusions and outlook

The first measurement of the impact-parameter dependence of the modulation of the ρ^0 yield with the ϕ angle in coherent photoproduction processes from Pb–Pb ultraperipheral collisions at a center-of-mass energy of $\sqrt{s_{\rm NN}} = 5.02$ TeV has been presented. The ρ^0 was detected using the ALICE detector through its decay into a pion pair and the observable ϕ is an azimuthal angle defined in Sec. 3.2. The impact parameter is estimated considering neutron emission at forward rapidity. A significant impact-parameter dependence of the anisotropy strength was observed, with the amplitude of the $\cos(2\phi)$ modulation increasing by about one order of magnitude from the 0n0n (no neutrons emitted, large impact parameter) to the XnXn (neutrons emitted by both colliding nuclei, relatively small impact parameter) class. This trend is well reproduced by the theoretical models [14, 33]. The results for the XnXn class are compatible with those, by the STAR Collaboration, for Au–Au and U–U collisions at RHIC.

The current experimental uncertainties do not allow the measurement to constrain the models, but this will become possible using the large data set that is being collected by ALICE during Run 3 and in the future Run 4 of the LHC. This large amount of data will also enable a more detailed characterization of the quantum interference effects, by means of more differential studies and the study of similar effects in other processes, such as the coherent photoproduction of the J/ψ, where the model predictions are expected to be more accurate.

References

[1] Gerhard Baur et al. "Coherent $\gamma\gamma$ and γA interactions in very peripheral collisions at relativistic ion colliders". In: *Phys.Rept.* 364 (2002), pp. 359–450. DOI: 10.1016/S0370-1573(01)00101-6. arXiv: hep-ph/0112211 [hep-ph].

[2] A. J. Baltz et al. "The Physics of Ultraperipheral Collisions at the LHC". In: *Phys. Rept.* 458 (2008). Ed. by G. Baur et al., pp. 1–171. DOI: 10.1016/j.physrep.2007.12.001. arXiv: 0706.3356 [nucl-ex].

[3] J. G. Contreras and J. D. Tapia Takaki. "Ultra-peripheral heavy-ion collisions at the LHC". In: *Int. J. Mod. Phys.* A30 (2015), p. 1542012. DOI: 10.1142/S0217751X15420129.

[4] Spencer R. Klein and Heikki Mäntysaari. "Imaging the nucleus with high-energy photons". In: *Nature Rev. Phys.* 1 (2019), pp. 662–674. DOI: 10.1038/s42254-019-0107-6. arXiv: 1910.10858 [hep-ex].

[5] Spencer R. Klein and Joakim Nystrand. "Interference in exclusive vector meson production in heavy ion collisions". In: *Phys. Rev. Lett.* 84 (2000), pp. 2330–2333. DOI: 10.1103/PhysRevLett.84.2330. arXiv: hep-ph/9909237.

[6] Anthony J. Baltz, Spencer R. Klein, and Joakim Nystrand. "Coherent vector meson photoproduction with nuclear breakup in relativistic heavy ion collisions". In: *Phys. Rev. Lett.* 89 (2002), p. 012301. DOI: 10.1103/PhysRevLett.89.012301. arXiv: nucl-th/0205031.

[7] I. A. Pshenichnov et al. "Mutual heavy ion dissociation in peripheral collisions at ultrarelativistic energies". In: *Phys. Rev. C* 64 (2001), p. 024903. DOI: 10.1103/PhysRevC.64.024903. arXiv: nucl-th/0101035.

[8] I. A. Pshenichnov. "Electromagnetic excitation and fragmentation of ultrarelativistic nuclei". In: *Phys. Part. Nucl.* 42 (2011), pp. 215–250. DOI: 10.1134/S1063779611020067.

[9] M. Broz, J. G. Contreras, and J. D. Tapia Takaki. "A generator of forward neutrons for ultra-peripheral collisions: $\mathbf{n_O^O n}$". In: *Comput. Phys. Commun.* (2020), p. 107181. ISSN: 0010-4655. DOI: https://doi.org/10.1016/j.cpc.2020.107181. arXiv: 1908.08263 [nucl-th].

[10] Spencer R. Klein et al. "STARlight: A Monte Carlo simulation program for ultra-peripheral collisions of relativistic ions". In: *Comput. Phys. Commun.* 212 (2017), pp. 258–268. DOI: 10.1016/j.cpc.2016.10.016. arXiv: 1607.03838 [hep-ph].

[11] Cong Li, Jian Zhou, and Ya-Jin Zhou. "Probing the linear polarization of photons in ultraperipheral heavy ion collisions". In: *Phys. Lett. B* 795 (2019), pp. 576–580. DOI: 10.1016/j.physletb.2019.07.005. arXiv: 1903.10084 [hep-ph].

[12] Cong Li, Jian Zhou, and Ya-Jin Zhou. "Impact parameter dependence of the azimuthal asymmetry in lepton pair production in heavy ion collisions". In: *Phys. Rev. D* 101 (2020), p. 034015. DOI: 10.1103/PhysRevD.101.034015. arXiv: 1911.00237 [hep-ph].

[13] Jaroslav Adam et al. "Measurement of e^+e^- Momentum and Angular Distributions from Linearly Polarized Photon Collisions". In: *Phys. Rev. Lett.* 127 (2021), p. 052302. DOI: 10.1103/PhysRevLett.127.052302. arXiv: 1910.12400 [nucl-ex].

[14] Hongxi Xing et al. "The cos 2ϕ azimuthal asymmetry in ρ^0 meson production in ultraperipheral heavy ion collisions". In: *JHEP* 10 (2020), p. 064. DOI: 10.1007/JHEP10(2020)064. arXiv: 2006.06206 [hep-ph].

[15] Wangmei Zha et al. "Exploring the double-slit interference with linearly polarized photons". In: *Phys. Rev. D* 103 (2021), p. 033007. DOI: 10.1103/PhysRevD.103.033007. arXiv: 2006.12099 [hep-ph].

[16] Mohamed Abdallah et al. "Tomography of ultrarelativistic nuclei with polarized photon-gluon collisions". In: *Sci. Adv.* 9 (2023), eabq3903. DOI: 10.1126/sciadv.abq3903. arXiv: 2204.01625 [nucl-ex].

[17] "Azimuthal Correlations within Exclusive Dijets with Large Momentum Transfer in Photon-Lead Collisions". In: *Phys. Rev. Lett.* 131 (5 Aug. 2023), p. 051901. DOI: 10.1103/PhysRevLett.131.051901. arXiv: 2205.00045 [hep-ex].

[18] K. Aamodt et al. "The ALICE experiment at the CERN LHC". In: *JINST* 3 (2008), S08002. DOI: 10.1088/1748-0221/3/08/S08002.

[19] Betty Abelev et al. "Performance of the ALICE Experiment at the CERN LHC". In: *Int. J. Mod. Phys.* A29 (2014), p. 1430044. DOI: 10.1142/S0217751X14300440. arXiv: 1402.4476 [nucl-ex].

[20] K Aamodt et al. "Alignment of the ALICE Inner Tracking System with cosmic-ray tracks". In: *JINST* 5 (2010), P03003. DOI: 10.1088/1748-0221/5/03/P03003. arXiv: 1001.0502 [physics.ins-det].

[21] J. Alme et al. "The ALICE TPC, a large 3-dimensional tracking device with fast readout for ultra-high multiplicity events". In: *Nucl. Instrum. Meth.* A622 (2010), pp. 316–367. DOI: 10.1016/j.nima.2010.04.042. arXiv: 1001.1950 [physics.ins-det].

[22] E. Abbas et al. “Performance of the ALICE VZERO system”. In: *JINST* 8 (2013), P10016. DOI: 10.1088/1748-0221/8/10/P10016. arXiv: 1306.3130 [nucl-ex].

[23] K Akiba et al. “LHC forward physics”. In: *Journal of Physics G: Nuclear and Particle Physics* 43.11 (Oct. 2016), p. 110201. DOI: 10.1088/0954-3899/43/11/110201. URL: https://dx.doi.org/10.1088/0954-3899/43/11/110201.

[24] Shreyasi Acharya et al. “Coherent photoproduction of ρ^0 vector mesons in ultra-peripheral Pb–Pb collisions at $\sqrt{s_{\rm NN}} = 5.02$ TeV”. In: *JHEP* 06 (2020), p. 035. DOI: 10.1007/JHEP06(2020)035. arXiv: 2002.10897 [nucl-ex].

[25] J. Adam et al. “Coherent ρ^0 photoproduction in ultra-peripheral Pb–Pb collisions at $\sqrt{s_{\rm NN}} = 2.76$ TeV”. In: *Journal of High Energy Physics* 9 (2015). ISSN: 1029-8479. URL: http://dx.doi.org/10.1007/JHEP09(2015)095.

[26] Spencer R. Klein and Joakim Nystrand. “Exclusive vector meson production in relativistic heavy ion collisions”. In: *Phys. Rev.* C60 (1999), p. 014903. DOI: 10.1103/PhysRevC.60.014903. arXiv: hep-ph/9902259 [hep-ph].

[27] L. C. Maximon and R. A. Schrack. “The form factor of the Fermi model spatial distribution”. In: *J. Res. Natl. Bur. Stand. B* 70.1 (1966), pp. 85–94. DOI: 10.6028/jres.070b.007.

[28] Allan S. Krass. “Interference Effects in Photoproduction of ϱ^0 Mesons”. In: *Phys. Rev.* 159 (5 1967), pp. 1496–1500. DOI: 10.1103/PhysRev.159.1496.

[29] R. L. Workman et al. “Review of Particle Physics”. In: *PTEP* 2022 (2022), p. 083C01. DOI: 10.1093/ptep/ptac097.

[30] Marc Ross and Leo Stodolsky. “Photon Dissociation Model for Vector-Meson Photoproduction”. In: *Phys. Rev.* 149 (4 1966), pp. 1172–1181. DOI: 10.1103/PhysRev.149.1172.

[31] Yoshikazu Hagiwara et al. “Coulomb nuclear interference effect in dipion production in ultraperipheral heavy ion collisions”. In: *Phys. Rev. D* 103 (2021), p. 074013. DOI: 10.1103/PhysRevD.103.074013. arXiv: 2011.13151 [hep-ph].

[32] Gerhard Baur et al. “Multiphoton exchange processes in ultraperipheral relativistic heavy ion collisions”. In: *Nucl. Phys. A* 729 (2003), pp. 787–808. DOI: 10.1016/j.nuclphysa.2003.09.006. arXiv: nucl-th/0307031.

[33] Heikki Mäntysaari et al. *Effects of nuclear structure and quantum interference on diffractive vector meson production in ultra-peripheral nuclear collisions*. 2023. arXiv: 2310.15300 [nucl-th]. URL: https://arxiv.org/abs/2310.15300.

[34] Francois Gelis et al. “The Color Glass Condensate”. In: *Ann. Rev. Nucl. Part. Sci.* 60 (2010), pp. 463–489. DOI: 10.1146/annurev.nucl.010909.083629. arXiv: 1002.0333 [hep-ph].

[35] Carlos A. Bertulani and Gerhard Baur. “Electromagnetic processes in relativistic heavy ion collisions”. In: *Physics Reports* 163.5 (1988), pp. 299–408. ISSN: 0370-1573. DOI: https://doi.org/10.1016/0370-1573(88)90142-1.

[36] A. J. Baltz, M. J. Rhoades-Brown, and J. Weneser. “Heavy-ion partial beam lifetimes due to Coulomb induced processes”. In: *Phys. Rev. E* 54 (4 1996), pp. 4233–4239. DOI: 10.1103/PhysRevE.54.4233.

[37] A. J. Baltz and Mark Strikman. “Suppression of heavy ion $\gamma\gamma$ production of the Higgs particle by Coulomb dissociation”. In: *Phys. Rev. D* 57 (1 1998), pp. 548–549. DOI: 10.1103/PhysRevD.57.548.